Bioorganic Chemistry 87 (2019) 200–208

Contents lists available at ScienceDirect

Bioorganic Chemistry

journal homepage: www.elsevier.com/locate/bioorg

Development of a versatile DNMT and HDAC inhibitor **C02S** modulating multiple cancer hallmarks for breast cancer therapy

Zigao Yuan[a,b,1], Shaopeng Chen[b,c,1], Chunmei Gao[b,d], Qiuzi Dai[b], Cunlong Zhang[b], Qinsheng Sun[b], Jin-Shun Lin[b], Chun Guo[a], Yuzong Chen[b,e], Yuyang Jiang[a,b,f,*]

[a] Department of Pharmaceutical Engineering, Shenyang Pharmaceutical University, Shenyang, Liaoning 110016, PR China
[b] National & Local United Engineering Lab for Personalized Anti-tumor Drugs, Shenzhen Kivita Innovative Drug Discovery Institute, The Graduate School at Shenzhen, Tsinghua University, Shenzhen 518055, PR China
[c] Health Science Center, Shenzhen University, Shenzhen 518060, PR China
[d] College of Chemistry and Chemical Engineering, Shenzhen University, Shenzhen 518060, PR China
[e] Department of Pharmacy, Faculty of Science, National University of Singapore, 117543, Singapore
[f] Department of Pharmacology and Pharmaceutical Sciences, School of Medicine, Tsinghua University, Beijing 100084, PR China

ARTICLE INFO

Keywords:
Epigenetic
DNMT
HDAC
Dual inhibitor
Cancer therapy

ABSTRACT

DNMT and HDAC are closely related to each other and involved in various human diseases especially cancer. These two enzymes have been widely recognized as antitumor targets for drug discovery. Besides, research has indicated that combination therapy consisting of DNMT and HDAC inhibitors exhibited therapeutic advantages. We have reported a DNMT and HDAC dual inhibitor **15a** of which the DNMT enzymatic inhibitory potency needs to be improved. Herein we reported the development of a novel dual DNMT and HDAC inhibitor **C02S** which showed potent enzymatic inhibitory activities against DNMT1, DNMT3A, DNMT3B and HDAC1 with IC_{50} values of 2.05, 0.93, 1.32, and 4.16 μM, respectively. Further evaluations indicated that **C02S** could inhibit DNMT and HDAC at cellular levels, thereby inversing mutated methylation and acetylation and increasing expression of tumor suppressor proteins. Moreover, **C02S** regulated multiple biological processes including inducing apoptosis and G0/G1 cell cycle arrest, inhibiting angiogenesis, blocking migration and invasion, and finally suppressing tumor cells proliferation *in vitro* and tumor growth *in vivo*.

1. Introduction

Alterations of epigenetic modifications (e.g., DNA methylation and histone modifications) play important roles in the initiation and progression of human cancers, providing attractive biomarkers and targets for diagnostic and therapeutic purposes [1–5]. Generally, epigenetic control is involved in all of the hallmarks of tumorigenesis and survival (e.g., sustaining proliferation, inducing angiogenesis, activating invasion and metastasis) [6,7], therefore epigenetic therapy can concurrently modulate and reverse multiple aberrant signaling pathways, inducing widespread changes in gene expression and multiple antitumor biological processes [8]. In the past few years, targeting epigenetic variation to reverse epigenome abnormalities has been widely recognized as a practical therapeutic strategy for cancer and other human disease such as inflammation, neurological, autoimmune and cardiovascular diseases [9–12].

DNA methyltransferases (DNMTs) and histone deacetylases (HDACs), which separately catalyze the methylation of CpG islands in DNA and deacetylation in histones and other substrate proteins, are the most studied and recognized epigenetic targets for antitumor agents discovery [13–17]. Now two DNMT inhibitors (DNMTi) (i.e., azacytidine and decitabine) and five HDAC inhibitors (HDACi) (i.e., vorinostat, depsipeptide, belinostat, panobinostat, and chidamide) have been approved for cancer therapy. The abnormalities of DNMT and HDAC are both linked to the decreased expression of tumor suppressor genes (TSGs) in human cancers. Besides, DNMT and HDAC are closely related in cellular biology [18–21]. The interplay of DNA methylation and histone de-acetylation reinforces the silence of TSGs and poses a challenge for the durability of DNMTi and HDACi used as single agents, attributing to that either aberration could be the dominant driver for tumorigenesis and survival [22]. It has been reported that DNA methylation may give rise to acquired resistance for HDACi [23]. On the

* Corresponding author at: Department of Pharmaceutical Engineering, Shenyang Pharmaceutical University, Shenyang, Liaoning 110016, PR China.
E-mail address: jiangyy@sz.tsinghua.edu.cn (Y. Jiang).
[1] Authors with equal contributions.

https://doi.org/10.1016/j.bioorg.2019.03.027
Received 18 February 2019; Received in revised form 13 March 2019; Accepted 13 March 2019
Available online 19 March 2019
0045-2068/

other hands, researches demonstrated that combination therapies consisting of DNMTi and HDACi showed significant synergistic antitumor effect, including suppressing the tumorigenicity of cancer stem-like cells and enhancing cancer immune therapy [24–28]. Hence we proposed that developing multi-target inhibitors against DNMT and HDAC simultaneously might be an alternative approach for cancer treatments.

Multitarget drugs might overcome resistance and improve outcomes *vs* single-target agents, and have more predictable pharmacokinetic (PK) and pharmacodynamic (PD) and lower toxicities *vs* drug combinations [29–33]. As a part of our ongoing development of multitarget antitumor agents [34–38], we previously reported compound **15a** as a DNMT and HDAC dual inhibitor with potent HDAC inhibitory activity and potential DNMT inhibitory potency [39]. In the present study, we designed and synthesized a novel DNMT and HDAC dual inhibitor, **C02S**, based on rational drug design strategy. Our data documented that **C02S** had good DNMT/HDAC enzymatic inhibitory potency and significant antitumor activity against breast cancer cells by modulating multiple cancer hallmarks, warranting **C02S** as a promising antitumor lead compound.

2. Rational design and synthesis

Generally, HDAC inhibitors share similar pharmacophore characteristics consisting of three groups: a cap group to occlude the entrance of the active site pocket; a zinc-binding group (ZBG) to chelate the zinc ion in the active catalytic site; and a linker to connect the cap group and ZBG [31,39]. On the other hand, DC-517 and its *S*- and *R*-enantiomers are selective DNMT1 inhibitors reported by Luo's group [40] with IC_{50} values of 1.7, 2.5, 1.8 μM, respectively. These compounds consist of two carbazole groups and a side chain, within which the hydroxyl group is critical to form an essential hydrogen bond interaction with DNMT1. Herein we intend to introduce the hydroxamic acid group to the end of the side chain, with not changing the carbazole groups and the hydroxyl group. In our opinion, our target compounds **C02** and its enantiomers (*R*)-**C02** and (*S*)-**C02** possess the general functional group characteristics of HDACi warranting them to be potential HDAC inhibitors; besides, the similar molecular scaffold with DC-517 would be helpful to bind with DNMT (Scheme 1).

The synthesis of target compound (*RS*)-**C02** is illustrated as Scheme 2. Compound (*RS*)-**3** was synthesized as reported procedures [40] and then reacted with ethyl piperidine-4-carboxylate to yield (*RS*)-**C01**, which subsequently was converted to target molecule (*RS*)-**C02** by performing a nucleophilic substitution reaction. Similarly, (*R*)-epichlorohydrin and (*S*)-epichlorohydrin separately reacted with compound **2** to give (*R*)-**3** and (*S*)-**3** [40], respectively, which were finally converted to (*R*)-**C02** (**C02R**) and (*S*)-**C02** (**C02S**) under the same conditions (supporting data, Scheme S1 and S2).

3. Results and discussion

3.1. *C02S* suppressed tumor cells proliferation

To evaluate the antitumor potency of our compounds, we firstly conducted an MTT assay, with the approved HDAC inhibitor SAHA and the DNMT inhibitor SGI-1027 used as reference compounds. As shown in Table 1, compound **C02S** exhibited more potent antiproliferative potency than that of SAHA and SGI-1027 in tumor cells MCF-7, A549 and MDA-MB-231 with IC_{50} values of 1.88, 3.92 and 4.65 μM, respectively. Compounds **C02** and **C02R** showed weak inhibitory activities against MCF-7 with IC_{50} values more than 20 μM and barely inhibited A549 proliferation, whereas presented comparable proliferation inhibitory potency against MDA-MB-231 cells with that of SAHA and SGI-1027. Taken together, these results suggest that **C02S** might be a potential antitumor agent, and we chose **C02S** to perform further biological activity evaluations, given that **C02S** displayed the most potent antiproliferative potency in the tested tumor cells.

3.2. *C02S* is a potent dual DNMT and HDAC inhibitor

We then investigate the enzymatic inhibitory potency of **C02S** against DNMT and HDAC. As we expected, the results (Fig. 1) indicated **C02S** potently inhibited DNMT1 with an IC_{50} value of 2.05 μM, which is comparable with DC-517. Besides, unlike DC-517 which only inhibited DNMT1 but not DNMT3A or DNMT3B, **C02S** also exhibited significant inhibitory potencies against DNMT3A and DNMT3B with IC_{50} values of 0.93 and 1.32 μM, respectively, suggesting that the side chain modification of DC-517 might be critical for its selectivity towards DNMT1 over DNMT3A and DNMT3B. HDAC1 and HDAC6 have been recognized to be critical in breast cancer cells [41]. Further HDAC inhibition assay indicated that **C02S** is a moderate HDAC1 inhibitor with an IC_{50} value of 4.16 μM, but showed no inhibitory activity against HDAC6 (IC_{50} > 100 μM, data not shown). Taken together, the enzymatic inhibitory activities of **C02S** indicate our feasible design of dual DNMT and HDAC inhibitor by merging functional groups of DNMT inhibitor DC-517 with hydroxamic acid HDAC inhibitors.

3.3. *C02S* regulated DNMT and HDAC activities in tumor cells

To further characterize the enzymatic inhibitory properties of **C02S** against DNMT and HDAC simultaneously, we further performed

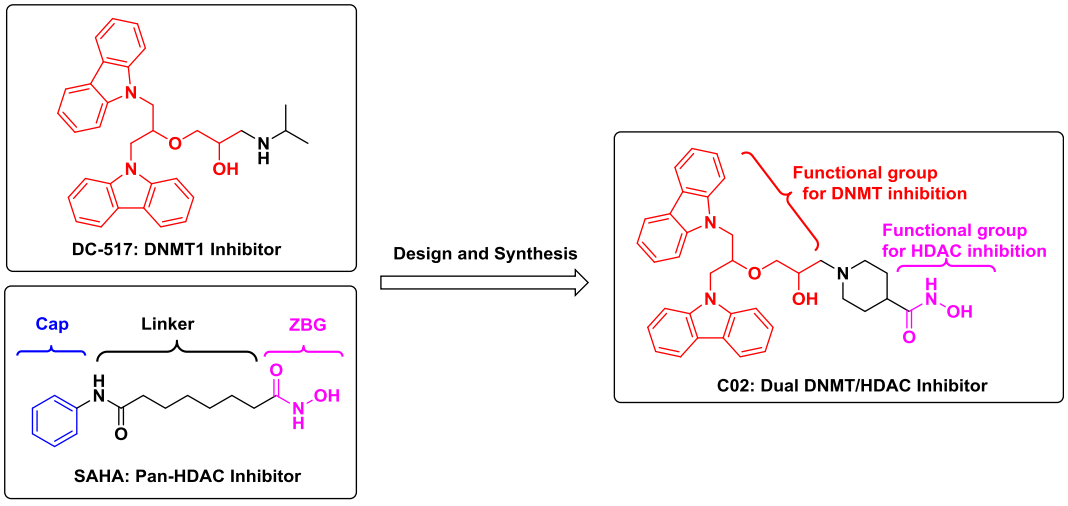

Scheme 1. Design of the hybrid compound **C02** as a proposed dual DNMT and HDAC inhibitor.

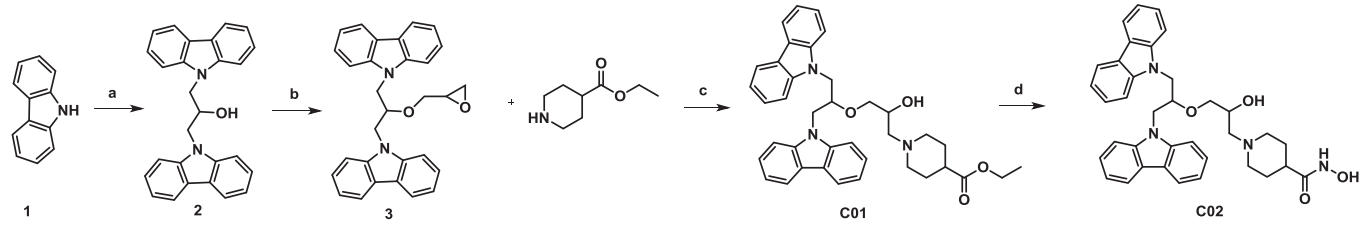

Scheme 2. Synthesis of designed dual DNMT and HDAC inhibitor **C02**. Reagent and conditions: (a) 1-Bromo-2,3-epoxypropane, NaH, DMF; (b) epichlorohydrin, KOH, Na_2SO_4, DMF; (c) EtOH, reflux; (d) NH_2OH, $NaOCH_3$, CH_3OH.

Table 1
Antiproliferative activities of compounds against tumor cells MCF-7, A549, and MDA-MB-231 (IC_{50}[a], μM).

	SAHA	SGI-1027	C02	C02R	C02S
MCF-7	7.89	5.01	20.22	29.70	1.88
A549	5.35	20.77	> 50	> 50	3.92
MDA-MB-231	9.33	7.45	8.98	7.94	4.65

[a] Data are expressed as the mean values of at least triplicate determinations with SD values < 10% of the mean values.

western blot assays to explore proteins expression. As shown in Fig. 2A, C02S treatments for 24 h induced DNMT1 degradation in a dose-dependent manner in MCF-7 cells, but barely influenced the expression of DNMT3A and DNMT3B. Besides, our results indicated that the expressions of tumor suppressor proteins TIMP3 and p16, which could be down-regulated at tumor cells due to the hypermethylation of promoter regions [42], were increased in MCF-7 cells after treated with **C02S** at defined concentrations.

To get further insight into the mechanism of reexpression of p16 in MCF-7 cells, we conducted a methylation-specific PCR (MS-PCR) assay to investigate whether the reexpression of p16 was due to the demethylation of *p16* CpG islands in MCF-7 cells. As shown in Fig. 2B, the promoter region of *p16* was hypermethylated in the blank control group (DMSO), which was consistent with the low-expression of p16. After treated with **C02S** at increasing concentrations from 1 to 3 μM for 36 h, a substantial amplification of unmethylated *p16* was observed, resulting in the increased expression of p16 in protein level as detected in Fig. 2A. These results indicated that **C02S** could suppress DNMTs activity at the cellular level and reverse methylation states of TSGs, thereby increasing the expression of tumor suppressor proteins.

Further assays revealed that treatment with **C02S** in MCF-7 cells improved the acetylation level of integral histone 3, as well as induced the hyperacetylation of H3K9 and H4K8 (Fig. 2A), demonstrating that **C02S** is an effective HDAC inhibitor at the cellular level. In addition, consistent with reported studies that HDAC inhibitor could cause DNA damages and increase the expression of p21 [43,44], **C02S** prompted DNA damages as the remarkable up-regulation of γ-H2AX (a specific biomarker for DNA double stands breaks) was observed (Fig. 2A). **C02S** also significantly induced the re-expression of tumor suppressor protein p21 in MCF-7 cells (Fig. 2A), which was reported to be associated with blockade of tumor cell cycle progression. These results demonstrated

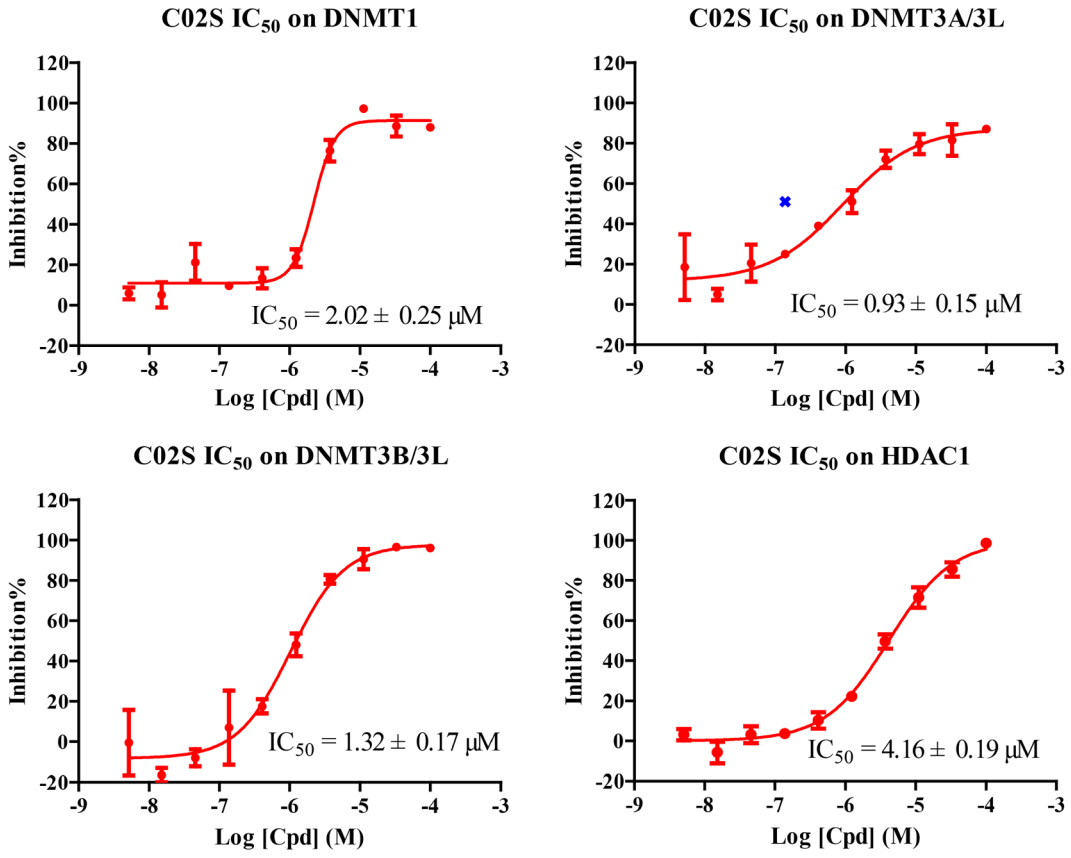

Fig. 1. Enzymatic inhibitory activities of **C02S** against DNMT1, DNMT3A, DNMT3B and HDAC1.

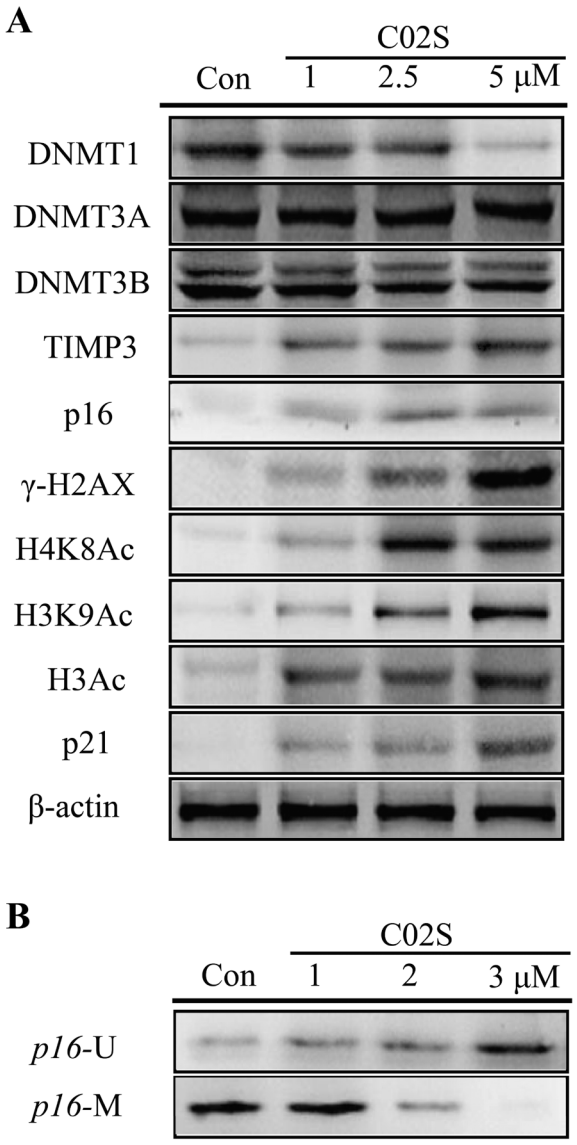

Fig. 2. **C02S** showed DNMT and HDAC inhibitory potency at cellular levels. (**A**) **C02S** induced DNMT1 degradation, increased histones H4K8, H3K9, and H3 hyperacetylation, upregulated the expression of tumor suppressor proteins TIMP3, p16 and p21, and caused DNA double-strand damages. (**B**) Compound **C02S** induced demethylation of *p16* CpG islands.

that **C02S** concurrently suppressed inhibitory activities of DNMT and HDAC at cellular levels and displayed collective antitumor advantages of DNMTi and HDACi.

3.4. *C02S caused G0/G1 cell cycle arrest in MCF-7 cells*

To evaluate whether **C02S** could induce tumor cell cycle arrest, we then performed a flow cytometry assay to assess the effect of **C02S** on the distribution of cell cycle. The cell cycle profiles of MCF-7 after treating with **C02S** in different concentrations for 48 h were illustrated in Fig. 3A. The G0/G1-phase fraction was gradually increased from 35.79% in the untreated cells to 47.25%, 51.62% and 56.36% in cells treated with **C02S** at 1, 2.5, and 5 μM, respectively, indicating that **C02S** caused G0/G1 cell cycle arrest in a dose-dependent manner. This consequence might partially result from the re-expression of p21 induced by **C02S**.

3.5. *C02S induced tumor cells apoptosis*

To further value the antitumor and growth-inhibitory effects of **C02S**, we then performed a PI-FITC/annexin assay to assess the proapoptosis ability of **C02S** in MCF-7 cells. As shown in Fig. 3B, 3.88% apoptotic cells were observed in control group treated with DMSO, whereas tumor cells treated with **C02S** at defined concentrations of 1, 2.5, and 5 μM for 48 h resulted in 10.18%, 90.08% and 95.47% cells apoptosis, respectively. Together with cell cycle analysis, these results suggested that **C02S** could inhibit tumor cells proliferation by inducing G0/G1 cell cycle arrest and prompting apoptosis.

3.6. *C02S possessed antiangiogenesis activity*

The process of inducing angiogenesis is a critical hallmark for tumors to supply sustenance and evacuate metabolite, and thus help sustain expanding neoplastic growth and invasion. Angiogenesis inhibitors (such as VEGF signaling inhibitors) have been widely explored in mechanism-based targeted therapy for cancer [7,45,46]. Given that epigenetic therapy could be involved in the cancer hallmark of angiogenesis, herein we next evaluated the effect of **C02S** on angiogenic behavior of HUVECs. The results (Fig. 4A) in the tube formation assay showed that **C02S** treatments significantly inhibited HUVEC tubule formation in a dose-dependent manner, suggesting that **C02S** possessed remarkable antiangiogenesis potency, which might attribute to the collective inhibition of DNMT and HDAC.

3.7. *C02S inhibited tumor cells migration and invasion*

We next examined whether **C02S** could suppress cancer cells migration using a wound healing assay. As the breast cancer cell line MDA-MB-231 is highly aggressive, invasive, and closely associated with poor prognosis, herein we chose MDA-MB-231 cells to perform the scratch assay. The results (Fig. 4B) indicated that treatment with **C02S** at concentrations of 1, 2.5, and 5 μM for 30 h induced significant dose-dependent inhibition of migration of MDA-MB-231 cells compared with DMSO control group.

We further performed a transwell experiment to assess the invasion inhibitory activity of **C02S** against tumor cells. In consistent with the wound healing assay, **C02S** potently blocked the invasion of MDA-MB-231 at defined concentrations (Fig. 4C). These results revealed that **C02S** could suppress migration and invasion of aggressive tumor cells.

3.8. *C02S suppressed tumor growth in vivo*

Given the observed multiple antitumor properties (proapoptosis, inducing cell cycle arrest, antiangiogenesis, and inhibiting migration and invasion) of **C02S**, we finally evaluate the *in vivo* activity of **C02S** against tumor growth using mice xenograft 4T1 breast tumor models which closely mimics late stage human breast cancer. The two drug groups were treated with **C02S** at dose of 5 mg/kg/d and 15 mg/kg/d, respectively, compared with the black control group treated with 2% DMSO solution and the positive control group treated with combination therapy consisting of SAHA (25 mg/kg/d) and decitabine (2.5 mg/kg/d). The results revealed that **C02S** treatments significantly reduced tumor volume and mass compared to DMSO group (Fig. 5). Although at lower dose, the drug group treated with **C02S** at dose of 15 mg/kg/d exhibited comparable tumor growth inhibitory potency with the positive control group treated with SAHA and decitabine (Fig. 5B–D). The average tumor volume and weight after sacrificed for **C02S** (15 mg/kg/d) *vs* positive control group were 0.13 *vs* 0.12 cm^3 (Fig. 5C), and 0.95 *vs* 0.74 g (Fig. 5D), respectively. Besides, no remarkable weight loss was observed in all tested mice (Fig. 5C), indicating the absence of side toxicity of drug groups. All these results indicated that **C02S** could effectively inhibit tumor growth *in vivo*.

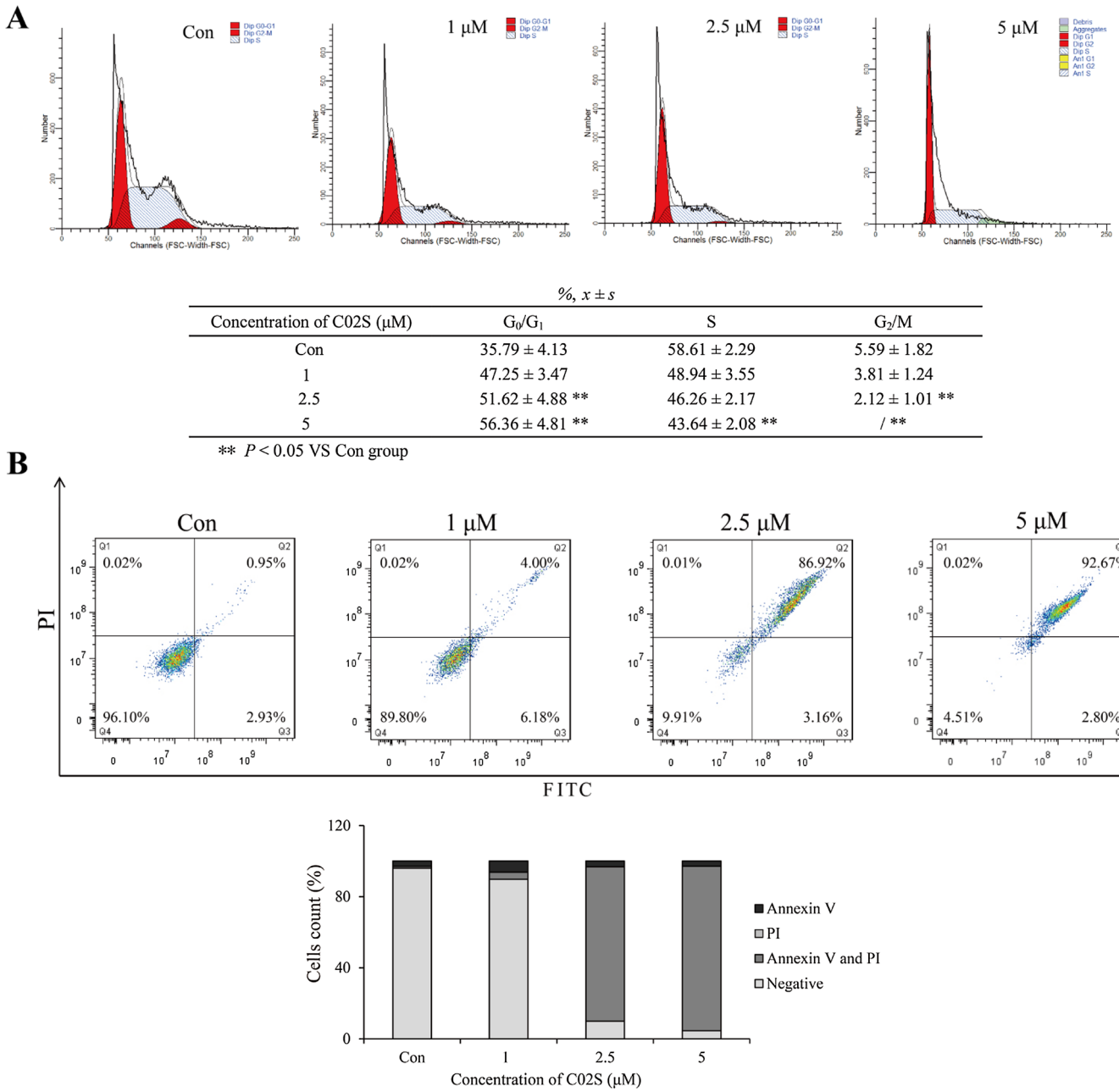

%, $x \pm s$

Concentration of C02S (μM)	G_0/G_1	S	G_2/M
Con	35.79 ± 4.13	58.61 ± 2.29	5.59 ± 1.82
1	47.25 ± 3.47	48.94 ± 3.55	3.81 ± 1.24
2.5	51.62 ± 4.88 **	46.26 ± 2.17	2.12 ± 1.01 **
5	56.36 ± 4.81 **	43.64 ± 2.08 **	/ **

** $P < 0.05$ VS Con group

Fig. 3. C02S inhibited tumor cells proliferation by blocking cell cycle and prompting apoptosis. (**A**) **C02S** treatments resulted in G0/G1 cell cycle arrest in MCF-7 cells. (**B**) **C02S** induced dose-dependent apoptosis of MCF-7 cells.

4. Conclusion

Epigenetic therapy has been supposed to simultaneously modify various cancer hallmarks and modulate multiple aberrant signaling pathways. However, most reported researches on epigenetic drug discovery only focused on certain hallmarks or specific pathways. In this study, we designed and synthesized a novel dual DNMT and HDAC inhibitor **C02S** and thoroughly evaluated its biological effect on manifold cancer hallmarks (e.g., proliferation, antiangiogenesis, invasion and migration). Results warranted **C02S** as a versatile antitumor agent displaying multiple antitumor biological effects. Specifically, **C02S** potently inhibited DNMT1, DNMT3A, DNMT3B and HDAC1 with IC_{50} values of 2.05, 0.93, 1.32, and 4.16 μM, respectively. Moreover, **C02S** exhibited remarkable inhibitory potency against DNMT and HDAC at cellular levels, inducing DNMT1 degradation and histones hyperacetylation, thereby leading to demethylation of promoter regions of TSG *p16* and upregulation of tumor suppression proteins p16, p21 and TIMP3. Additionally, **C02S** induced DNA damages, caused G0/G1 cell cycle arrest, and prompted apoptosis in human breast cancer cells MCF-7. Besides, **C02S** showed remarkable antiangiogenesis ability, inhibited migration and invasion of aggressive breast cancer cells MDA-MB-231. What's more, **C02S** significantly inhibited proliferation of tumor cells MCF-7 and A549, and suppressed tumor growth in mice breast cancer models. Taken together, **C02S** induced multiple antitumor effects and affected various cancer hallmarks by inhibiting DNMT and HDAC simultaneously. Our results suggest that developing agents targeting DNMT and HDAC concurrently can be a practical strategy for cancer epigenetic therapy and compound **C02S** represents a promising lead compound for further development.

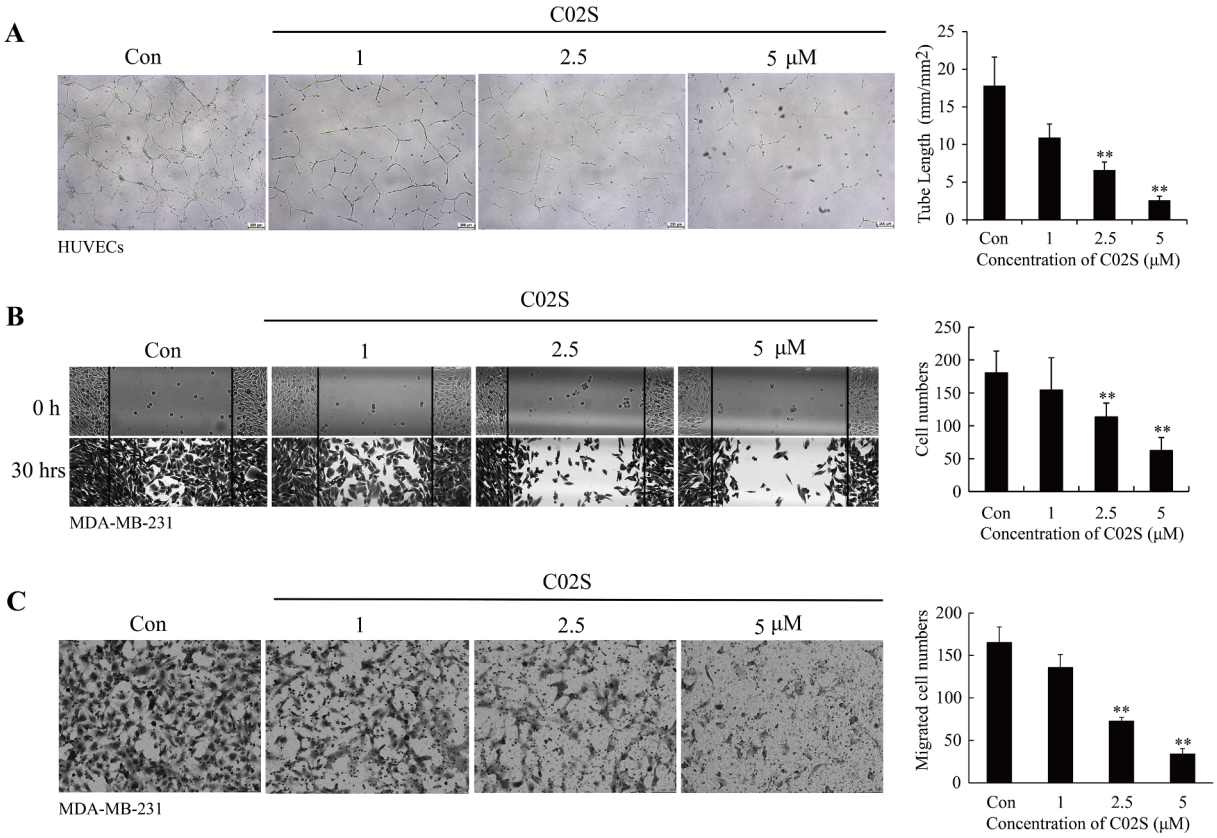

Fig. 4. C02S modulated multiple cancer hallmarks simultaneously, including inhibiting angiogenesis, invasion and migration. (**A**) **C02S** treatments reduced tube formation in HUVEC cells. (**B**) Wound healing assay and (**C**) transwell assay of **C02S** in MDA-MB-231 cells indicated **C02S** could suppress invasion and migration of aggressive tumor cells. $^{**}p < 0.01$.

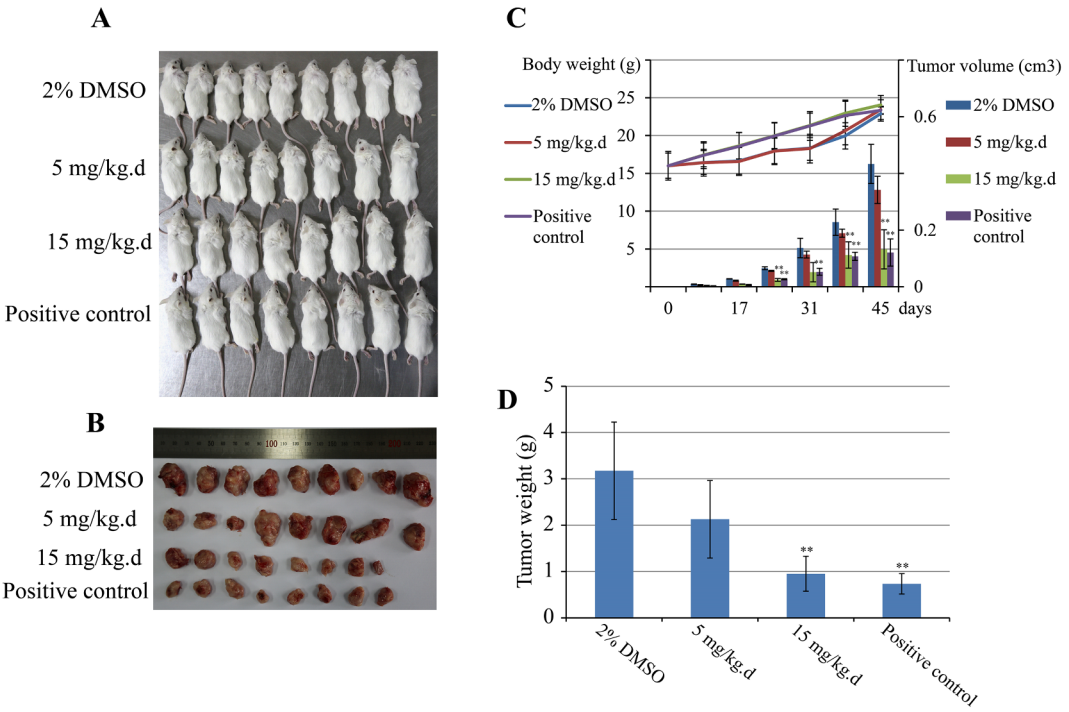

Fig. 5. In vivo antitumor activity of **C02S** against human breast cancer model in mice. (**A**) Image of tumor-bearing mice before anatomy; (**B**) Image of the internal tumor tissues after anatomy; (**C**) Relationship curves of mice weights and tumor volumes at various times (10 d, 17 d, 24 d, 31 d, 38 d, and 45 d) after administration; (**D**) Average mass of internal tumor tissues of mice after anatomy. Positive control: SAHA (25 mg/kg/d) and decitabine (2.5 mg/kg/d) co-treatments. $^{**}p < 0.01$.

5. Experimental section

5.1. Chemistry

Reagents and solvents were purchased from commercial sources and used without further purification. All anhydrous reactions were conducted under a nitrogen atmosphere. Nuclear magnetic resonance spectra were obtained using a Bruker 400 (400 MHz) spectrometer. Chemical shifts are given in ppm (δ) relative to $SiMe_4$ as internal standard. Coupling constants (J) are in hertz (Hz), and signals are designated as follows: s, singlet; d, doublet; t, triplet; m, multiplet; br, broad singlet, etc. The mass spectra were obtained on a Waters Micromass Q-TOF Premier Mass Spectrometer. Melting points were determined with a Hanon MP430 Melting Point Apparatus and are uncorrected. Enantiomeric excess (ee) was determined using Agilent high-performance liquid chromatography (HPLC) with a Hatachi detector (λ = 254 or 214 nm). Column conditions are reported in the experimental section below. All chemical yields are unoptimized and generally represent the result of a single experiment. Compound **3** [9,9′-(2-(oxiran-2-ylmethoxy)propane-1,3-diyl) -bis(9H-carbazole)] and its enantiomers (*R*)-**3** and (*S*)-**3** were synthesized following reported procedures [40], HPLC analysis for **3**: Chiralcel AD3 (*n*-hexane/i-PrOH = 95/5, flow rate 0.5 mL/min, λ = 254 nm), t_R (**3**) = 35.903/41.556 min, t_R ((***R***)-**3**) = 36.966 min, t_R ((***S***)-**3**) = 41.125 min.

5.1.1. General procedure for (RS)-*C01*, (R)-*C01* (*C01R*) and (S)-*C01* (*C01S*)

Compound (*RS*)-**3** (1 eq) and excess ethyl piperidine-4-carboxylate (4 eq) were added to ethanol in round flask, and then the mixture was heated to reflux until (*RS*)-**3** was consumed completely. The ethanol was removed by rotary evaporator and the residue was separated by column chromatography using gradient elution consisting of ethyl acetate and petroleum ether to obtain pure (*RS*)-**C01** as a white solid. Similarly, (*R*)-**3** and (*S*)-**3** separately reacted with ethyl piperidine-4-carboxylate to give (*R*)-**C01** and (*S*)-**C01**, respectively, under the same conditions.

*5.1.1.1. Ethyl 1-(3-((1,3-di(9H-carbazol-9-yl)propan-2-yl)oxy)-2-hydroxypropyl) -piperidine-4-carboxylate (**C01**).* Yield 65%; melting point 109–110 °C; ^{1}H NMR (400 MHz, $CDCl_3$) δ 8.11 (d, J = 8.3 Hz, 4H), 7.48–7.37 (m, 4H), 7.33–7.20 (m, 8H), 4.67–4.52 (m, 2H), 4.50–4.40 (m, 1H), 4.36 (t, J = 4.5 Hz, 1H), 4.32 (t, J = 4.5 Hz, 1H), 4.16 (q, J = 7.1 Hz, 2H), 3.39–3.25 (m, 1H), 3.10 (qd, J = 10.3, 4.8 Hz, 2H), 2.56–2.45 (m, 1H), 2.43–2.31 (m, 1H), 2.28–2.13 (m, 1H), 2.01–1.90 (m, 1H), 1.87–1.75 (m, 3H), 1.69–1.54 (m, 4H), 1.28 (t, J = 7.1 Hz, 3H); ^{13}C NMR (101 MHz, $CDCl_3$) δ 174.7, 140.5, 140.4, 126.0 (2C), 125.9, 123.1 (2C), 120.5, 120.4, 119.41 (2C), 108.9, 108.8, 78.3, 77.2, 73.9, 60.7, 60.4, 60.2, 53.6, 51.7, 45.7, 45.6, 40.6, 28.0, 27.8. HRMS (ESI) *m/z* calculated for $[M+H]^+$ 604.3175, found 604.3179. HPLC analysis for **C01**: Chiralcel IF3 (*n*-hexane/i-PrOH = 80/20, flow rate 0.4 mL/min, λ = 254 nm), t_R = 38.166/40.640 min.

*5.1.1.2. Ethyl (R)-1-(3-((1,3-di(9H-carbazol-9-yl)propan-2-yl)oxy)-2-hydroxypropyl) -piperidine-4-carboxylate (**C01R**).* Yield 71%; melting point 107–108 °C; ^{1}H NMR (400 MHz, $CDCl_3$) δ 8.14–8.04 (m, 4H), 7.44–7.34 (m, 4H), 7.29–7.19 (m, 8H), 4.63–4.50 (m, 2H), 4.47–4.37 (m, 1H), 4.33 (dd, J = 5.0, 3.5 Hz, 1H), 4.29 (dd, J = 4.9, 3.6 Hz, 1H), 4.12 (q, J = 7.1 Hz, 2H), 3.30–3.20 (m, 1H), 3.10–3.03 (m, 2H), 2.50–2.41 (m, 1H), 2.37–2.28 (m, 1H), 2.21–2.11 (m, 1H), 1.93–1.83 (m, 1H), 1.79–1.71 (m, 3H), 1.66–1.46 (m, 7H), 1.25 (t, J = 7.2 Hz, 3H); ^{13}C NMR (101 MHz, $CDCl_3$) δ 174.9, 140.5, 140.4, 125.9 (2C), 123.1 (2C), 120.5, 120.4, 119.4, 108.9, 108.8, 78.3, 77.3, 77.2, 77.0, 76.7, 74.0, 60.3, 60.0, 53.8, 51.7, 45.8, 45.7, 40.9, 28.3, 28.1. HPLC analysis: Chiralcel IF3 (*n*-hexane/i-PrOH = 80/20, flow rate 0.4 mL/min, λ = 254 nm), t_R = 38.353 min.

*5.1.1.3. Ethyl (S)-1-(3-((1,3-di(9H-carbazol-9-yl)propan-2-yl)oxy)-2-hydroxypropyl) -piperidine-4-carboxylate (**C01S**).* Yield 69%; melting point 108–109 °C; ^{1}H NMR (400 MHz, $CDCl_3$) δ 8.09 (d, J = 7.7 Hz, 4H), 7.44–7.35 (m, 4H), 7.29–7.19 (m, 8H), 4.63–4.52 (m, 2H), 4.48–4.37 (m, 1H), 4.34 (dd, J = 5.0, 3.5 Hz, 1H), 4.30 (dd, J = 4.9, 3.6 Hz, 1H), 4.12 (q, J = 7.1 Hz, 2H), 3.32–3.20 (m, 1H), 3.07 (d, J = 4.6 Hz, 2H), 2.50–2.43 (m, 1H), 2.36–2.30 (m, 1H), 2.26–2.07 (m, 1H), 1.94–1.83 (m, 1H), 1.78–1.69 (m, 3H), 1.64–1.55 (m, 7H), 1.25 (t, J = 7.1 Hz, 3H); ^{13}C NMR (101 MHz, $CDCl_3$) δ 175.0, 140.5 (2C), 125.9 (2C), 123.1 (2C), 120.5, 120.4, 119.4, 108.9, 108.8, 78.3, 77.2, 74.0, 60.3, 60.0, 53.8, 51.7, 45.8, 45.7, 41.0, 28.3, 28.1. HPLC analysis: Chiralcel IF3 (*n*-hexane/i-PrOH = 80/20, flow rate 0.4 mL/min, λ = 254 nm), t_R = 40.556 min.

5.1.2. General procedure for (RS)-*C02*, (R)-*C02* (*C02R*) and (S)-*C02* (*C02S*)

Compound (*RS*)-**C01** (1 eq) was added to methanol in round flask, and then NH_2OH aqueous (15.17 M, 5 eq) and $NaOCH_3$ solution in methanol (5 M, 10 eq) were added dropwise. The mixture was stirred at room temperature for 1 h, and then the solvent was removed by rotary evaporator. The solid was dissolved in water, then hydrochloric acid solution (3 M) was added to modulate pH to neutral. The resulting suspension was filtrated and washed with diethyl ether to provide the hydroxamic acid product (*RS*)-**C02**. Similarly, (*R*)-**C01** and (*S*)-**C01** were separately used as reaction reagent to product (*R*)-**C02** and (*S*)-**C02**, respectively. The products were characterized by ^{1}H NMR, ^{13}C NMR, melting point and high resolution mass spectrum (HRMS, ESI).

*5.1.2.1. 1-(3-((1,3-di(9H-carbazol-9-yl)propan-2-yl)oxy)-2-hydroxypropyl)-N-hydroxypiperidine-4-carboxamide (**C02**).* Yield 85%; melting point 170–172 °C; ^{1}H NMR (400 MHz, DMSO-d_6) δ 10.42 (s, 1H), 8.71 (s, 1H), 8.25–8.07 (m, 4H), 7.80–7.55 (m, 4H), 7.53–7.32 (m, 4H), 7.30–7.10 (m, 4H), 4.78–4.49 (m, 4H), 4.35–4.21 (m, 1H), 3.01–2.86 (m, 1H), 2.72–2.58 (m, 1H), 2.40–2.15 (m, 2H), 1.96–1.78 (m, 1H), 1.78–1.23 (m, 8H); ^{13}C NMR (101 MHz, DMSO-d_6) δ 170.8, 140.3, 140.2, 125.6, 122.1, 120.2, 118.9, 109.5, 77.9, 73.4, 60.0, 51.4, 45.0, 27.2. HRMS (ESI) *m/z* calculated for $C_{36}H_{38}N_4O_4$ $[M+H]^+$ 591.2971, found 591.2956.

*5.1.2.2. (R)-1-(3-((1,3-di(9H-carbazol-9-yl)propan-2-yl)oxy)-2-hydroxypropyl)-N-hydroxypiperidine-4-carboxamide (**C02R**).* Yield 87%; melting point 202–203 °C; ^{1}H NMR (400 MHz, DMSO-d_6) δ 10.52 (s, 1H), 8.76 (s, 1H), 8.35–8.00 (m, 4H), 7.84–7.56 (m, 4H), 7.56–7.33 (m, 4H), 7.33–7.06 (m, 4H), 4.79–4.56 (m, 4H), 4.40–4.18 (m, 1H), 3.04–2.90 (m, 1H), 2.75–2.61 (m, 1H), 2.45–2.32 (m, 2H), 2.06–1.28 (m, 9H); ^{13}C NMR (101 MHz, DMSO-d_6) δ 140.3, 140.2, 125.7, 122.1, 120.2, 119.0, 109.6, 109.5, 78.0, 73.1, 45.0. HRMS (ESI) *m/z* calculated for $C_{36}H_{38}N_4O_4$ $[M+H]^+$ 591.2971, found 591.2968.

*5.1.2.3. (S)-1-(3-((1,3-di(9H-carbazol-9-yl)propan-2-yl)oxy)-2-hydroxypropyl)-N-hydroxypiperidine-4-carboxamide (**C02S**).* Yield 92%; melting point 108–109 °C; ^{1}H NMR (400 MHz, DMSO-d_6) δ 10.31 (s, 1H), 8.65 (s, 1H), 8.24–8.00 (m, 4H), 7.68–7.49 (m, 4H), 7.49–7.28 (m, 4H), 7.28–7.05 (m, 4H), 4.82–4.62 (m, 2H), 4.62–4.39 (m, 2H), 4.36–4.18 (m, 1H), 3.71 (s, 1H), 2.93–2.82 (m, 1H), 2.73–2.61 (m, 1H), 2.25–2.06 (m, 2H), 1.81–1.65 (m, 1H), 1.56–1.15 (m, 8H); ^{13}C NMR (101 MHz, DMSO-d_6) δ 171.4, 140.3, 140.2, 125.6, 125.5, 122.1, 120.1, 118.8 (2C), 109.5, 77.8, 73.6, 66.4, 60.5, 53.2, 52.3, 45.0, 28.2, 28.1. HRMS (ESI) *m/z* calculated for $C_{36}H_{38}N_4O_4$ $[M+H]^+$ 591.2971, found 591.2997.

5.2. Biology

The *in vitro* enzymatic inhibitory potency of **C02S** against DNMTs and HDAC1/6 were tested by Shanghai Chempartner Co., Ltd in Shanghai, China, as we reported before [39]. The tumor cell lines MCF-

7, A549, MDA-MB-231, HUVEC, and 4T1 were purchased from the Cell Bank of Chinese Academy of Science (Shanghai, China) and cultured according to the supplier's protocol. Cell proliferation inhibition evaluation using an MTT assay, apoptosis detection and cell cycle analysis using flow cytometry, protein expression assessment using western blot, and methylation-specific PCR of *p16* were performed following protocols as we reported [37,39]. For MTT assay and enzymatic inhibition test, IC_{50} values with two decimal places were calculated from inhibitory curves generated by GraphPad Prism 5.

5.2.1. Antiangiogenesis assay

The tube formation assay was conducted following described protocol [47]. Briefly, aliquots (150 μL) of Matrigel (BD Biosciences) were added into a 48-well plate and incubated at 37 °C for 30 min. HUVEC cells were resuspended in collected supernatants from each pretreatment and then seeded onto the gel (2×10^4 cells/well). Cells were treated either vehicle or different concentrations of **C02S**. Five random fields in each well were chosen and photographed after 24 h. Networks of tube-like structures were measured using Image-Pro-Plus 6.0 software.

5.2.2. Wound healing assay

Wound-healing assay was modified from the standard scratch wound-healing assay as described by Liang et al [48]. MDA-MB-231 cells were seeded in 6-well plates at a density of 2×10^5 cells/mL, and the cells were serum starved with fetal bovine serum (FBS)-free medium for 12 h once reaching confluence. Three parallel lines were drawn on the bottom of the six-well plates before seeding cells and wounds were created by scratching with 200 μL sterile pipette tips vertically to the lines drawn. After washing and changing with fresh medium, the cells were treated with either vehicle or different concentrations of **C02S**. The wounds next to the lines were photographed at the beginning and 30 h after scratching under phase contrast microscope using the 10× objective lens. Cell numbers were counted by Image-Pro-Plus 6.0 software in the same area marked between the labeled lines and the wound.

5.2.3. Transwell evaluation

Cell invasion assay was performed as described [49,50]. Invasion inserts with 8 μm pore membranes from Corning (New York, USA) were coated with fibronectin from Sigma-Aldrich (Missouri, USA) as described [51]. MDA-MB-231 Cells were pretreated with vehicle or **C02S** at concentrations of 1, 2.5, and 5 μM for 6 h, respectively. The pretreated cells were seeded on the inserts to reach confluence in 12 h, and then culture for another 24 h with drug treatment. After fixed with 4% formaldehyde, non-invading cells on the upper side of the membranes were removed by cotton swab. The invading cells were stained with 0.08% trypan blue for 15 min and were photographed by a bright-field light microscope. Cell numbers of five random views were counted by Image-Pro-Plus 6.0 of Media Cybernetics (MD, USA).

5.2.4. In vivo antitumor activity assay

The *in vivo* antitumor evaluation of **C02S** against mouse models was approved by the Bioethics Committee of Graduate School at Shenzhen, Tsinghua university. We used 4T1 mouse model which closely mimics late stage human breast cancer to assess *in vivo* activity of **C02S** for breast cancer therapy. **C02S** was dissolved in DMSO (2%) and diluted with PBS. Twenty-eight female BALB/c mice (6–8 weeks, 16 ± 1 g each weigh) were divided into 4 groups (Black control treated with 2% DMSO, Positive control treated with 25 mg/kg/d of SAHA and 2.5 mg/kg/d of decitabine, and two experimental groups treated with **C02S** of 5 mg/kg/d and 15 mg/kg/d, respectively). All mice were fed a standard mouse pellet diet. The 4T1 cells were used for induction of tumors in inbred Balb/c mice. 200 μL of RPMI-containing 4T1 cells at concentration of 1×10^6 cells/mL was injected into the mammary glands of female mice. All mice were followed until a tumor nodule was observed. Tumor growth was measured twice a week by caliper measurement of the tumor length. The volume of each tumor was determined using the formula $V = 0.5 \times d^2 \times D$, where V is the tumor volume (cubic centimeter), d is the shorter diameter, and D is the longer diameter. The weight of mice was record weekly. Tumors (~0.2 cm diameter) were observed 1 week after cells seeding. Vehicle (0.2 mL of 2% DMSO), Positive control (25 mg/kg of SAHA and 2.5 mg/kg decitabine), 5 mg/kg (0.2 mL × 0.5 mg/mL of **C02S**) and 15 mg/kg/d (0.2 mL × 1.5 mg/mL of **C02S**) were injected to mice *via* i.p. once every day. The mice were sacrificed on day 45 after the initial treatment and the tumor tissues were harvested and weighed.

Acknowledgements

The authors would like to thank the financial supports from China Postdoctoral Science Foundation (2018M631825), Shenzhen Development and Reform Committee (20151961), and Department of Science and Technology of Guangdong Province (2017B030314083).

Conflict of interest

The authors declare no competing financial interests.

Appendix A. Supplementary material

Supplementary data (the ^1H NMR, ^{13}C NMR, HRMS, and HPLC of synthesized compounds) associated with this article can be found in the online version. Supplementary data to this article can be found online at https://doi.org/10.1016/j.bioorg.2019.03.027.

References

[1] S. Moran, A. Martinez-Cardus, S. Boussios, M. Esteller, Precision medicine based on epigenomics: the paradigm of carcinoma of unknown primary, Nat. Rev. Clin. Oncol. 14 (2017) 682–694.
[2] A. Koch, S.C. Joosten, Z. Feng, T.C. de Ruijter, M.X. Draht, V. Melotte, K.M. Smits, J. Veeck, J.G. Herman, L.V. Neste, W.V. Criekinge, T. De Meyer, M.V. Engeland, Analysis of DNA methylation in cancer: location revisited, Nat. Rev. Clin. Oncol. 15 (2018) 459–466.
[3] M.A. Dawson, The cancer epigenome: concepts, challenges, and therapeutic opportunities, Science 355 (2017) 1147–1152.
[4] D. Schuebeler, Function and information content of DNA methylation, Nature 517 (2015) 321–326.
[5] M. Widschwendter, A. Jones, I. Evans, D. Reiser, J. Dillner, K. Sundstrom, E.W. Steyerberg, Y. Vergouwe, O. Wegwarth, F.G. Rebitschek, U. Siebert, G. Sroczynski, I.D. de Beaufort, I. Bolt, D. Cibula, M. Zikan, L. Bjorge, N. Colombo, N. Harbeck, F. Dudbridge, A.M. Tasse, B.M. Knoppers, Y. Joly, A.E. Teschendorff, N. Pashayan, F.C. Consortium, Epigenome-based cancer risk prediction: rationale, opportunities and challenges, Nat. Rev. Clin. Oncol. 15 (2018) 292–309.
[6] H. Shen, P.W. Laird, Interplay between the cancer genome and epigenome, Cell 153 (2013) 38–55.
[7] D. Hanahan, R.A. Weinberg, Hallmarks of cancer: the next generation, Cell 144 (2011) 646–674.
[8] N. Azad, C.A. Zahnow, C.M. Rudin, S.B. Baylin, The future of epigenetic therapy in solid tumours–lessons from the past, Nat. Rev. Clin. Oncol. 10 (2013) 256–266.
[9] R.L. Bennett, J.D. Licht, Targeting epigenetics in cancer, Annu. Rev. Pharmacol. Toxicol. 58 (2018) 187–207.
[10] S.X. Pfister, A. Ashworth, Marked for death: targeting epigenetic changes in cancer, Nat. Rev. Drug. Discov. 16 (2017) 241–263.
[11] A.D. Kelly, J.-P.J. Issa, The promise of epigenetic therapy: reprogramming the cancer epigenome, Curr. Opin. Genet. Dev. 42 (2017) 68–77.
[12] R.A. Copeland, Epigenetic medicinal chemistry, ACS Med. Chem. Lett. 7 (2016) 124–127.
[13] K.J. Falkenberg, R.W. Johnstone, Histone deacetylases and their inhibitors in cancer, neurological diseases and immune disorders, Nat. Rev. Drug. Discov. 13 (2014) 673–691.
[14] C.H. Arrowsmith, C. Bountra, P.V. Fish, K. Lee, M. Schapira, Epigenetic protein families: a new frontier for drug discovery, Nat. Rev. Drug. Discov. 11 (2012) 384–400.
[15] C. Zagni, G. Floresta, G. Monciino, A. Rescifina, The search for potent, small-molecule HDACIs in cancer treatment: a decade after Vorinostat, Med. Res. Rev. 37 (2017) 1373–1428.
[16] D. Pechalrieu, C. Etievant, P.B. Arimondo, DNA methyltransferase inhibitors in cancer: from pharmacology to translational studies, Biochem. Pharmacol. 129 (2017) 1–13.
[17] A. Erdmann, L. Halby, J. Fahy, P.B. Arimondo, Targeting DNA methylation with small molecules: what's next? J. Med. Chem. 58 (2015) 2569–2583.

[18] F. Fuks, W.A. Burgers, A. Brehm, L. Hughes-Davies, T. Kouzarides, DNA methyltransferase Dnmt1 associates with histone deacetylase activity, Nat. Genet. 24 (2000) 88–91.
[19] K.D. Robertson, S. Ait-Si-Ali, T. Yokochi, P.A. Wade, P.L. Jones, A.P. Wolffe, DNMT1 forms a complex with Rb, E2F1 and HDAC1 and represses transcription from E2F-responsive promoters, Nat. Genet. 25 (2000) 338–342.
[20] M.R. Rountree, K.E. Bachman, S.B. Baylin, DNMT1 binds HDAC2 and a new corepressor, DMAP1, to form a complex at replication foci, Nat. Genet. 25 (2000) 269–277.
[21] T. Harada, H. Ohguchi, Y. Grondin, S. Kikuchi, M. Sagawa, Y.T. Tai, R. Mazitschek, T. Hideshima, K.C. Anderson, HDAC3 regulates DNMT1 expression in multiple myeloma: therapeutic implications, Leukemia 31 (2017) 2670–2677.
[22] P.A. Jones, S.B. Baylin, The epigenomics of cancer, Cell 128 (2007) 683–692.
[23] V.R. Fantin, V.M. Richon, Mechanisms of resistance to histone deacetylase inhibitors and their therapeutic implications, Clin. Cancer Res. 13 (2007) 7237–7242.
[24] M.J. Topper, M. Vaz, K.B. Chiappinelli, C.E. DeStefano Shields, N. Niknafs, R.-W.C. Yen, A. Wenzel, J. Hicks, M. Ballew, M. Stone, P.T. Tran, C.A. Zahnow, M.D. Hellmann, V. Anagnostou, P.L. Strissel, R. Strick, V.E. Velculescu, S.B. Baylin, Epigenetic therapy ties MYC depletion to reversing immune evasion and treating lung cancer, Cell 171 (2017) 1284–1300.e1221.
[25] R. Pathania, S. Ramachandran, G. Mariappan, P. Thakur, H. Shi, J.H. Choi, S. Manicassamy, R. Kolhe, P.D. Prasad, S. Sharma, Combined inhibition of DNMT and HDAC blocks the tumorigenicity of cancer stem-like cells and attenuates mammary tumor growth, Cancer Res. 76 (2016) 3224–3235.
[26] R.A. Juergens, J. Wrangle, F.P. Vendetti, S.C. Murphy, M. Zhao, B. Coleman, R. Sebree, K. Rodgers, C.M. Hooker, N. Franco, B. Lee, S. Tsai, I.E. Delgado, M.A. Rudek, S.A. Belinsky, J.G. Herman, S.B. Baylin, M.V. Brock, C.M. Rudin, Combination epigenetic therapy has efficacy in patients with refractory advanced non-small cell lung cancer, Cancer Discov. 1 (2011) 598–607.
[27] X.W. Yang, D.L. Phillips, A.T. Ferguson, W.G. Nelson, J.G. Herman, N.E. Davidson, Synergistic activation of functional estrogen receptor (ER)-alpha by DNA methyltransferase and histone deacetylase inhibition in human ER-alpha-negative breast cancer cells, Cancer Res. 61 (2001) 7025–7029.
[28] I. Ecke, F. Petry, A. Rosenberger, S. Tauber, S. Monkemeyer, I. Hess, C. Dullin, S. Kimmina, J. Pirngruber, S.A. Johnsen, A. Uhmann, F. Nitzki, L. Wojnowski, W. Schulz-Schaeffer, O. Witt, H. Hahn, Antitumor effects of a combined 5-aza-2'deoxycytidine and valproic acid treatment on rhabdomyosarcoma and medulloblastoma in Ptch mutant mice, Cancer Res. 69 (2009) 887–895.
[29] A. Ganesan, Multitarget drugs: an epigenetic epiphany, ChemMedChem 11 (2016) 1227–1241.
[30] A.R. de Lera, A. Ganesan, Epigenetic polypharmacology: from combination therapy to multitargeted drugs, Clin. Epigenet. 8 (2016) 105.
[31] J. Roche, P. Bertrand, Inside HDACs with more selective HDAC inhibitors, Eur. J. Med. Chem. 121 (2016) 451–483.
[32] Y. Bansal, O. Silakari, Multifunctional compounds: smart molecules for multifactorial diseases, Eur. J. Med. Chem. 76 (2014) 31–42.
[33] A. Anighoro, J. Bajorath, G. Rastelli, Polypharmacology: challenges and opportunities in drug discovery, J. Med. Chem. 57 (2014) 7874–7887.
[34] C. Ding, S. Chen, C. Zhang, G. Hu, W. Zhang, L. Li, Y.Z. Chen, C. Tan, Y. Jiang, Synthesis and investigation of novel 6-(1,2,3-triazol-4-yl)-4-aminoquinazolin derivatives possessing hydroxamic acid moiety for cancer therapy, Bioorg. Med. Chem. 25 (2017) 27–37.
[35] B. Chu, F. Liu, L. Li, C. Ding, K. Chen, Q. Sun, Z. Shen, Y. Tan, C. Tan, Y. Jiang, A benzimidazole derivative exhibiting antitumor activity blocks EGFR and HER2 activity and upregulates DR5 in breast cancer cells, Cell Death Dis. 6 (2015) e1686.
[36] C. Zhang, C. Tan, X. Zu, X. Zhai, F. Liu, B. Chu, X. Ma, Y. Chen, P. Gong, Y. Jiang, Exploration of (S)-3-aminopyrrolidine as a potentially interesting scaffold for discovery of novel Abl and PI3K dual inhibitors, Eur. J. Med. Chem. 46 (2011) 1404–1414.
[37] Z. Yuan, S. Chen, C. Chen, J. Chen, C. Chen, Q. Dai, C. Gao, Y. Jiang, Design, synthesis and biological evaluation of 4-amidobenzimidazole acridine derivatives as dual PARP and Topo inhibitors for cancer therapy, Eur. J. Med. Chem. 138 (2017) 1135–1146.
[38] Z. Cui, S. Chen, Y. Wang, C. Gao, Y. Chen, C. Tan, Y. Jiang, Design, synthesis and evaluation of azaacridine derivatives as dual-target EGFR and Src kinase inhibitors for antitumor treatment, Eur. J. Med. Chem. 136 (2017) 372–381.
[39] Z. Yuan, Q. Sun, D. Li, S. Miao, S. Chen, L. Song, C. Gao, Y. Chen, C. Tan, Y. Jiang, Design, synthesis and anticancer potential of NSC-319745 hydroxamic acid derivatives as DNMT and HDAC inhibitors, Eur. J. Med. Chem. 134 (2017) 281–292.
[40] S. Chen, Y. Wang, W. Zhou, S. Li, J. Peng, Z. Shi, J. Hu, Y.C. Liu, H. Ding, Y. Lin, L. Li, S. Cheng, J. Liu, T. Lu, H. Jiang, B. Liu, M. Zheng, C. Luo, Identifying novel selective non-nucleoside DNA methyltransferase 1 inhibitors through docking-based virtual screening, J. Med. Chem. 57 (2014) 9028–9041.
[41] C. Tang, C. Li, S. Zhang, Z. Hu, J. Wu, C. Dong, J. Huang, H.-B. Zhou, Novel bioactive hybrid compound dual targeting estrogen receptor and histone deacetylase for the treatment of breast cancer, J. Med. Chem. 58 (2015) 4550–4572.
[42] J. Datta, K. Ghoshal, W.A. Denny, S.A. Gamage, D.G. Brooke, P. Phiasivongsa, S. Redkar, S.T. Jacob, A new class of quinoline-based DNA hypomethylating agents reactivates tumor suppressor genes by blocking DNA methyltransferase 1 activity and inducing its degradation, Cancer Res. 69 (2009) 4277–4285.
[43] C.B. Yoo, P.A. Jones, Epigenetic therapy of cancer: past, present and future, Nat. Rev. Drug. Discov. 5 (2006) 37–50.
[44] A. Scuto, M. Kirschbaum, C. Kowolik, L. Kretzner, A. Juhasz, P. Atadja, V. Pullarkat, R. Bhatia, S. Forman, Y. Yen, R. Jove, The novel histone deacetylase inhibitor, LBH589, induces expression of DNA damage response genes and apoptosis in Ph- acute lymphoblastic leukemia cells, Blood 111 (2008) 5093–5100.
[45] G.C. Jayson, R. Kerbel, L.M. Ellis, A.L. Harris, Antiangiogenic therapy in oncology: current status and future directions, Lancet 388 (2016) 518–529.
[46] Y. Shan, B. Wang, J. Zhang, New strategies in achieving antiangiogenic effect: Multiplex inhibitors suppressing compensatory activations of RTKs, Med. Res. Rev. (2018), https://doi.org/10.1002/med.21517.
[47] I. Arnaoutova, J. George, H.K. Kleinman, G. Benton, The endothelial cell tube formation assay on basement membrane turns 20: state of the science and the art, Angiogenesis 12 (2009) 267–274.
[48] C.C. Liang, A.Y. Park, J.L. Guan, In vitro scratch assay: a convenient and inexpensive method for analysis of cell migration in vitro, Nat. Protoc. 2 (2007) 329–333.
[49] D. Shan, L. Chen, D. Wang, Y.C. Tan, J.L. Gu, X.Y. Huang, The G protein G alpha(13) is required for growth factor-induced cell migration, Dev. Cell 10 (2006) 707–718.
[50] S. Yang, X.Y. Huang, Ca2+ influx through L-type Ca2+ channels controls the trailing tail contraction in growth factor-induced fibroblast cell migration, J. Biol. Chem. 280 (2005) 27130–27137.
[51] N. Wang, S.P. Chen, B. Zhang, S.F. Li, F. Jin, D. Gao, H.X. Liu, Y.Y. Jiang, 8u, a pro-apoptosis/cell cycle arrest compound, suppresses invasion and metastasis through HSP90 alpha downregulating and PI3K/Akt inactivation in hepatocellular carcinoma cells, Sci. Rep. 8 (2018), https://doi.org/10.1038/s41598-41017-18701-41593.